Molecular Dynamics Study on Ion Diffusion in $LiFePO_4$ Olivine Materials

Peixin Zhang,*,† Yanpeng Wu,† Dongyun Zhang,‡,§ Qiming Xu,§ Jianhong Liu,† Xiangzhong Ren,† Zhongkuan Luo,† Mingliang Wang,† and Weiliang Hong†

School of Chemistry and Chemical Engineering, Shenzhen University, Shenzhen 518060, P.R. China, School of Chemistry and Chemical Engineering, Guangxi University, Nanning 530004, P.R. China, and School of Materials Science and Engineering, Xi'an University of Architecture and Technology, Xi'an 710055, P.R. China

Received: October 22, 2007; Revised Manuscript Received: March 24, 2008

Molecular dynamics (MD) simulations have been employed to investigate the ionic diffusion and the structure of $LiFePO_4$ cathode material. The results correspond well with the published experimental observations. The simulation results indicated that the diffusion of lithium ions was thermally activated and more significant than those of other ions. Compared with other cathode materials, the shifts of ions were less significant in $LiFePO_4$. This suggested that $LiFePO_4$ was more thermally stable. The snapshots of the positions of lithium atoms over a range of the steps provided a microscopic picture and the picture showed the lithium ions migrated through one-dimension channels.

1. Introduction

Lithium secondary batteries have important applications in commercial electronics such as laptop computers, cell phones and cameras, and quite likely in hybrid electric vehicles (HEV). Emphasis has been changed dramatically since 1997 with the discovery of the electrochemical properties of the olivine phase $LiFePO_4$, in particular, by Padhi et al.[1] This is the first cathode material with potentially low cost, plentiful elements, large theoretical capacity (170 (mA h)/g) and also environmental friendly. However, this cathode may be affected by a loss of capacity with increasing charge/discharge current density and is low in electronic and ionic conductivity.[1,2] The low conductivity at room temperature is caused by the low lithium diffusion at the interface in two-phase $LiFePO_4/FePO_4$ system.[3,4]

As the key drawback in using $LiFePO_4$ is its low intrinsic electronic conductivity, many studies have been conducted in an attempt to solve this problem. Ravet et al.[5] showed that a carbon coating significantly improves the electrochemical performance of this material. Many other studies have been conducted on finding means to improve the electronic conductivity of the $LiFePO_4$ particles, such as adding conductive copper/silver powders, dispersing carbon black with high surface area, doping super valence cations, and synthesizing of small grains. In particular, Chung et al.[6] showed that the conductivity was increased by 8 orders of magnitude when $LiFePO_4$ was "doped" with aliovalent ions (e.g., Mg^{2+}, Zr^{4+}, Ti^{4+}, Al^{3+}, Nb^{5+}). However, it seems that the enhanced electronic conductivity does not improve the electrochemical performance as expected. Intrinsic ionic diffusivity may become quite relevant.

As the lithium ions undergo diffusion in the cathode materials during the charge and discharge processes, the MD (molecular dynamics) method is believed to be an efficient tool for understanding the structural features and the ion migration behavior. Molecular simulations have the advantage of bypassing some aspects of the experimental difficulties. It is clear that underlying transport properties of oxide cathode materials are complicated on the atomic scale but are crucial to better understanding of their structure−property relationship and electrochemical behavior. Regarding the ion diffusion in solid electrolytes, numerous theoretical studies, especially MD simulations, have been performed to investigate the ion diffusions and migration properties, as the MD method yields detailed information about migration pathways and temperature dependence.

The first-principles method,[7] the MC method[8] and the MD method[9–12] have been employed to carry out an estimation for the average voltage, energy density, the possibility of metal reduction and other properties of the cathode materials for lithium secondary batteries. As far as we know, only a few MD studies have focused on $LiFePO_4$ olivine materials by now. This research work focused on the structural, transport and other relevant properties of the $LiFePO_4$. The possible pathways for lithium ions migration obtained from the MD have been compared with the results from the first-principles method.

2. Computational Details

The interaction pair potential between ions i and j consists of a short-range term, the long-range Coulombic term and van der Waals interactions. These short-range interactions were modeled using the Buckingham potential:[9,13]

$$V_{ij}(r_{ij}) = A \exp(-r_{ij}/\rho) - Cr_{ij}^{\ 2} \qquad (1)$$

where A, ρ, and C are the Buckingham potential parameters and r is the interatomic distance. In addition to these two-body terms, the three-body term was also used in this work to control the O−P−O angle. Its takes the form of a harmonic angle-bending potential about the central P ion:

$$V_{3\text{-body}} = 1/2k(\theta - \theta_0)^2 \qquad (2)$$

where θ_0 is the tetrahedral angle (109.47°) and k is the bending force constant. This potential has been applied in the modeling of silicates,[14] aluminosilicates(zeolites)[15] and apatite materials[16–18] where account was taken of the angle-dependent nature of the SiO_4 or PO_4 tetrahedral units. For $LiFePO_4$, the potential parameters were derived simultaneously by empirical fitting to the observed crystal properties; this procedure generated a

* Corresponding author. E-mail: pxzhang96@yahoo.com.
† Shenzhen University.
‡ Guangxi University.
§ Xi'an University of Architecture and Technology.

10.1021/jp710204z CCC: $40.75
Published on Web 05/21/2008

TABLE 1: Two-Body Potential Parameters for $LiFePO_4$

interaction	A (eV)	ρ (Å)	C (eV Å^6)
Li−O	632.1018	0.2906	0.0
Fe−O	1105.2409	0.3106	0.0
P−O	897.2648	0.3577	0.0
O−O	22764.3	0.149	44.53

TABLE 2: Three-Body Potential Parameters for $LiFePO_4$

bonds	k (eV rad^{-2})	θ_0 (deg)
O−P--O	1.35578	109.47

TABLE 3: Core−Shell Harmonic Potential

interaction	K (eV Å^{-2})	Y (e)
Fec−Fes	19.27	2.986
Oc−Os	65.0	−2.96

TABLE 4: Input Fractional Coordinates of $LiFePO_4$ (*Pnma*)′ Structural Parameters for Calculations

ion	x	y	z
Li	0	0	0
P	0.0950	0.25	0.418
Fe core	0.2822	0.25	0.9738
Fe shell	0.2822	0.25	0.9738
O(1) core	0.09713	0.25	0.7428
O(1) shell	0.09713	0.25	0.7428
O(2) core	0.4573	0.25	0.2067
O(2) shell	0.4573	0.25	0.2067
O(3) core	0.166	0.0464	0.2851
O(3) shell	0.166	0.0464	0.2851

common set of interatomic potentials which are listed in Tables 1–3. Previous studies[19] have shown that these models reproduce adequately the crystal properties of $LiFePO_4$.

The dipolar shell model is proved to be very useful in modeling oxide materials[13,20] as it allows the polarization of ions in an electric field to be mimicked. In this study, the shell model for the oxygen and iron ions was used. In the dipolar shell model,[21] the total charge Z of the ion is split between a core (of charge $Z-Y$) and a shell (of charge Y), which are coupled by a harmonic spring k_{cs}.

$$E_{cs}(r) = 1/2 \times k_{cs} r^2 \tag{3}$$

Short-range forces only act on the shells, whereas Coulomb forces act on both shells and cores. The shells are then polarized by the field of the surrounding ions and the local environment of each ion affects its charge distribution.[21] In this approach, a small fraction of the core mass (0.2 au for oxygen and iron in this work) is assigned to the shell, and their motion, which is controlled by conventional equations of motion, follows the ionic motion adiabatically.

The MD simulations reported here were performed using the DL_POLY code,[22] in which the core−shell dynamics is controlled using the adiabatic shell method. The short-range potential and the real space component of Ewald summation were truncated at 8 and 12 Å and cubic periodic boundary conditions were implemented in all directions. The MD cell contained 756 atoms in total, specifically 108 Li, 108 Fe, 108 P and 432 O. The calculations were performed at temperatures of 300, 400, 600, 800 and 1200 K. The fractional coordinates of the starting structure used as observables[23] are listed in Table 4. Temperature and pressure were controlled by scaling the atom velocities and unit cell parameters, respectively. The calculations were performed using an NPT ensemble with a time step of 0.2 fs for 200000 steps, i.e., 40 ps in total. Equilibration runs

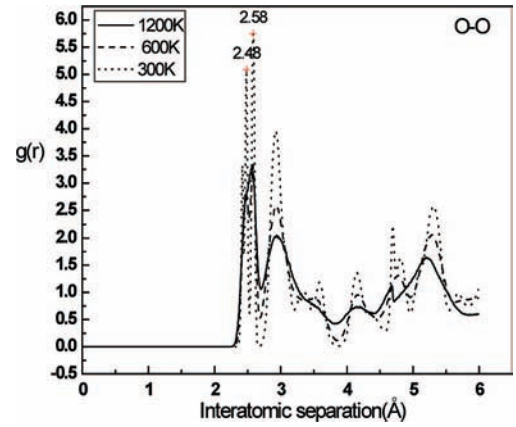

Figure 1. Radial distribution functions of O−O at different temperatures.

for 20 ps before the final production of running 20 ps, of which the last 100000 steps were used for statistical analysis at the last of 10∼20 ps in the final production. Temperature variations during the last run were less than 0.5% of the simulated temperature and the energy fluctuations were at most 0.1% around the mean value.

3. Results and Discussion

3.1. Structural Properties of $LiFePO_4$. The equilibrium structure of $LiFePO_4$ was measured by the radial distribution function (RDF) $g(r)$ that describes the spatial organization of ions about a central ion in the $LiFePO_4$ lattice. The radial distribution function was evaluated from the simulation data by using the fact that the average number of ions separated by a distance in the interval $[r, r + \triangle r]$ is related to $g(r)$:[24]

$$g_{ij}(r) = \frac{V}{N_i N_j} \sum_{i=1}^{N_{ij}} \frac{n_{ij}}{4\pi r^2 \Delta r} \tag{4}$$

where V is the volume of a unit cell, N_i and N_j are the number of atoms i and j, n_{ij} is the mean number of atoms in a shell of width between radius r and radius $r + \triangle r$ centered on the atom i. The method need not be restricted to one atom. All the atoms in the system can be treated in this way, leading to an improved determination of the RDF as an average over many atoms. At regular intervals, a snapshot of the system is taken and the number of atoms found in each shell is counted and stored. We can calculate the atomic radius in the molecular systems such as liquids, crystals, thus providing a direct comparison between experiment and simulation to evaluate the validity of the model.

We first obtained the O−O pair functions and the Fe−O radial distribution function from room temperature to a temperature which is near melting point. The results are shown in Figures 1 and 2, respectively. These plots show a series of well-defined peaks corresponding to successive nearest-neighbor distances, which are normal behavior for an ordered solid, especially at low temperature. These plots show that the peaks are sharp at low temperatures and become broad at high temperatures, indicating the thermal motion. They are particularly sharp in crystalline materials, where atoms are strongly confined in their positions. Figures 1 and 2 reveal that the first peak decreases in height as temperature increases from 300 to 1200 K, and the general profile broadens, indicating a greater degree of disorder at higher temperatures. This suggests that the ions move farther away from their lattice positions at higher temperatures. The decrease of height and broadening of these peaks is mainly due to the volume expansion of the crystalline $LiFePO_4$. Figures 3

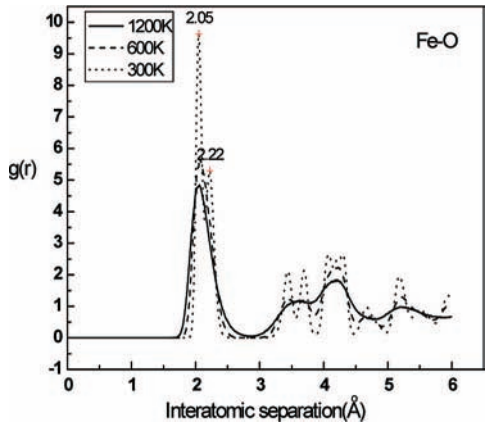

Figure 2. Radial distribution functions of Fe−O at different temperatures.

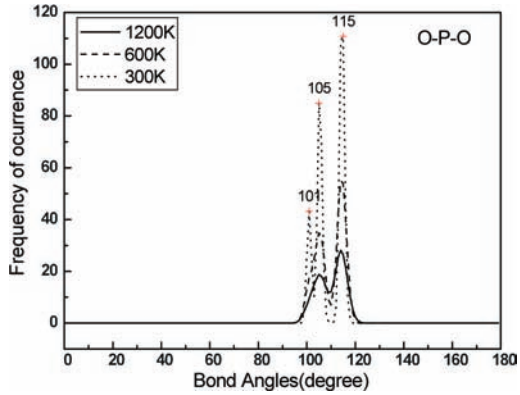

Figure 3. Angle correlation function of O−P−O bond angle in $LiFePO_4$ from MD simulation.

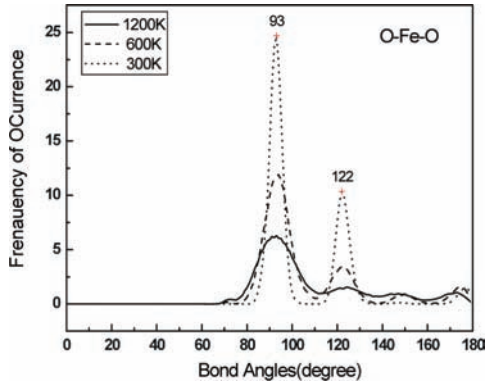

Figure 4. Angle correlation function of O−Fe−O bond angle in $LiFePO_4$ from MD simulation.

and 4 show the angle correlation function of O−P−O and O−Fe−O bond angles at different temperatures, respectively. From these plots, we note that the basic features of the plots about angle correlation function are very similar with the plots of RDF for all the temperatures considered between 300 and 1200 K.

We estimated the atomic radia and the bond angles from these plots at 300 K. Froms Figure 1 and 2, we calculated the atomic radius of O−O and Fe−O, and the bond angles O−P−O and O−Fe−O from Figures 3 and 4. The resulting data and experimental structural parameters from ref 23 are listed in Tables 5 and 6. Our calculated structural parameters are in good agreement with the experimental data. The simulations show

TABLE 5: Calculated and Experimental[23] Bond Lengths

ion pair	calcd (Å)	exptl (Å)	Δ (Å)
O(1)−O(2)	2.58	2.548	−0.054
O(1)−O(3)	2.58	2.536	−0.064
O(2)−O(3)	2.48	2.453	−0.027
Fe(1)−O(2)	2.05	2.085	0.035
Fe(1)−O(3)	2.22	2.095	−0.125

TABLE 6: Calculated and Experimental[23] Bond Angles

ion trimer	calcd (deg)	exptl (deg)	Δ (deg)
O(3)−P−O(1)	101	114.43	−3.43
O(3)−P−O(2)	105	105.71	0.71
O(3)−P−O(3)	105	104.46	−0.54
O(1)−P−O(2)	115	111.29	−3.71
O(2)−Fe−O(3)	93	89.01	−3.09
O(3)−Fe−O(3)	122	120.05	−1.95

good reproduction of the observed complex structure of $LiFePO_4$, which supports the validity of the potentials used for MD calculations.

3.2. Ion Diffusion. To investigate the diffusive properties of each species, their mean square displacements (MSDs) were calculated as a function of time for each composition.[24] The mean square displacements of the constituent atoms as a function of time t were calculated from their coordinates $r(t)$ with respect to the original positions at $t = t_0$ (Figure 7).

$$\mathrm{msd}(t) = \overline{|r(t) - r(t_0)|^2} \tag{5}$$

where the over line upon the right equation represents the average over all the atoms of the same species in the MD cell. The msd's of Li at various temperatures are shown in Figure 5. The value become constant after a short relaxation time for

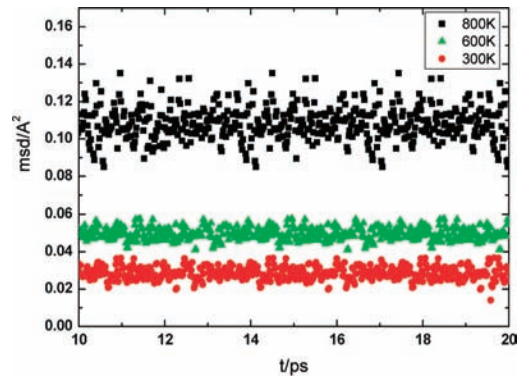

Figure 5. Mean square displacements of Li in $LiFePO_4$ at various temperatures as a function of time.

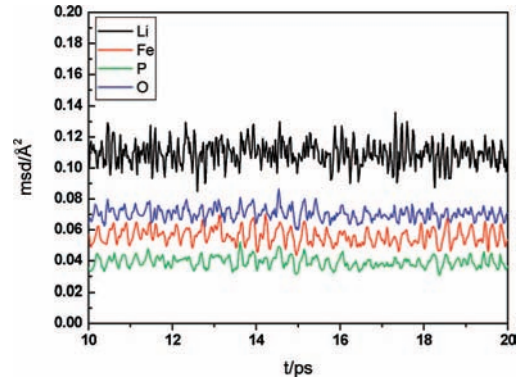

Figure 6. Mean square displacements of ions in $LiFePO_4$ at 300 K after relaxation.

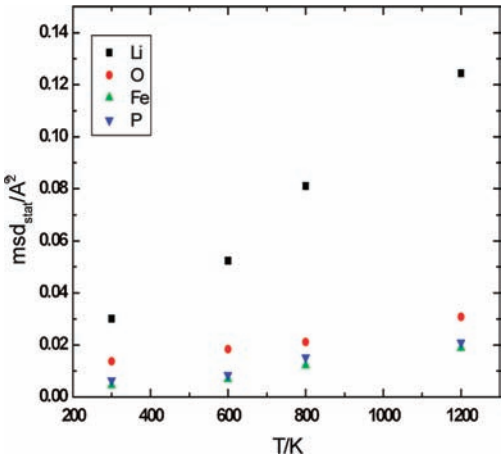

Figure 7. Changes of static components of the mean square displacement in $LiFePO_4$ with temperature.

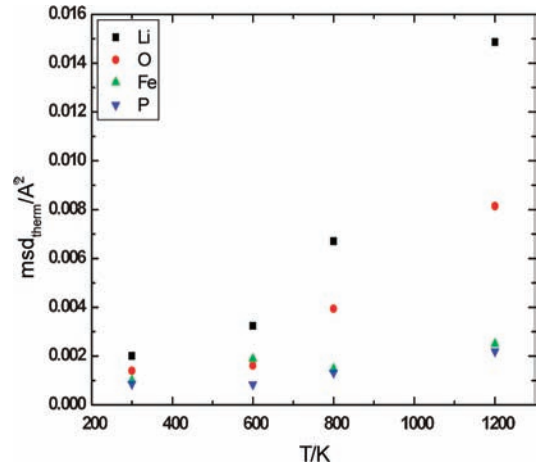

Figure 8. Changes of thermal components of the mean square displacement in $LiFePO_4$with temperature.

approximately 10 ps. Figure 5 reveals that the msd value is greater at the higher temperatures from 300 to 800 K and the distribution is more scattered at higher temperatures. In crystalline materials, atoms are strongly confined to their positions, and the ions can move farther away from their lattice positions at higher temperatures. The msd of Li at 600 K about 0.05 is far less than 0.6, the results of Tateishi et al.[25] The thermal stability of $LiFePO_4$ is critical to the application to cathode materials. It was observed that $LiFePO_4$ has no thermal excursions in its cells. This suggests that $LiFePO_4$ is more thermally stable compared to other cathode materials such as $LiMn_2O_4$.

Figure 6 shows the msd of all the ions at 300 K between 10 and 20 ps. The msd of Li is far larger than other ions in $LiFePO_4$. This suggests that the diffusivity of Li is much greater than the diffusivity of other ions. The same behavior was predicted by other studies. And this property is believed to be associated with the capability of electrochemical intercalation and deintercalation of the lithium ion of such materials.

When we calculated the msd from using eq 7, this msd_{therm} term includes the relaxation phase to distribute atoms statistically among various stable positions near the ideal positions and the early stage of the MD simulation. msd_{stat} is calculated to estimate these initial offsets as what follows.

$$msd_{stat} = \overline{\langle |\langle r(t)\rangle_{stat} - r(t_0)|^2 \rangle} \quad (6)$$

The msd_{therm} mainly arises from the thermal fluctuation of atoms after relaxation, and the formula is as follows:

$$msd_{therm} = \overline{\langle |r(t) - \langle r(t)\rangle_{stat}|^2 \rangle} \quad (7)$$

where the time-average surrounded by the angle brackets with subscript stat was taken over the time interval 10−20 ps for all atoms in the MD cell.

Figures 7 and 8 show the msd_{stat} and the msd_{therm} values at different temperatures, respectively. These figures indicate that msd_{stat} is a major component of the overall msd value. The msd_{therm}'s of all ions are proportional to temperature. On the other hand, the increase of the Li msd_{therm} contains a higher order component and the value of Li msd is higher than others. It reveals that the lithium ions were affected more by temperature change and more readily move away from the ideal position. The opportunity that ions hop through the channels increases at a higher temperature.

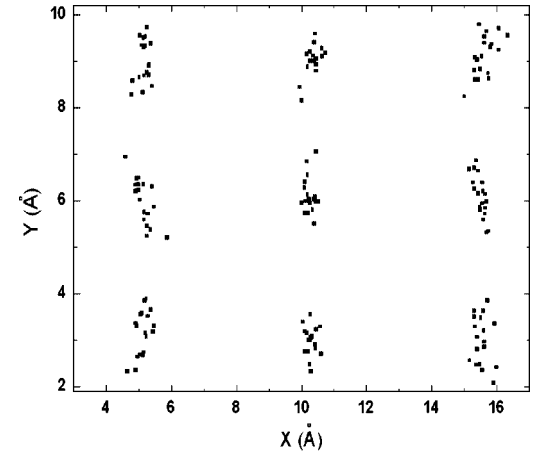

Figure 9. Snapshots of the movement of lithium atoms in the *XY* planes.

3.3. Migration Pathway. Examination of the intrinsic lithium ion mobility in $LiFePO_4$ is of vital interest when considering its use as a cathode material in lithium batteries. The unraveling of mechanistic detail at the microscopic level, which can be difficult from purely experimental studies, is a powerful feature of the MD technique.

To gain further insight into the migration mechanism, we have obtained "trajectory plots" which reveal the evolution of the ions. Figures 9 and 10 show the snapshots of the movement of lithium atoms projected in the *XY* and *YZ* planes between 11 and 20 ps every 200 steps. The trajectory plots exhibit that the diffusion distribution of lithium ions mainly exist in a narrow rectangle region and the diffusion process is anisotropic. The diffusion process was found to be one-dimensional, occurring along the channels parallel to the *y* axis, which was showed as arrow in Figure 11. In Figures 9 and 10 the lithium ions exhibit significant ion motion and the diffusion of ions spread of points between adjacent lattice sites along linear. With the increase of temperature, lithium can diffuse more easily by hoping along the *b* axis. Lithium diffusion is two-dimensional in $LiCoO_2$[26] and three-dimensional in $LiMn_2O_4$.[27] A lithium diffusion channel in $LiFePO_4$ is not quite clear from the experimental standpoint. Using the first-principle methods, Morgan et al.[7] found that Li diffuses through one-dimensional channels. Islam et al.[19] found that the pathway having the lowest lithium migration energy is along the $[010]_{pnma}$ channel. Ouyang et al.[28] reported similar results. The present study has obtained similar results. Ad-

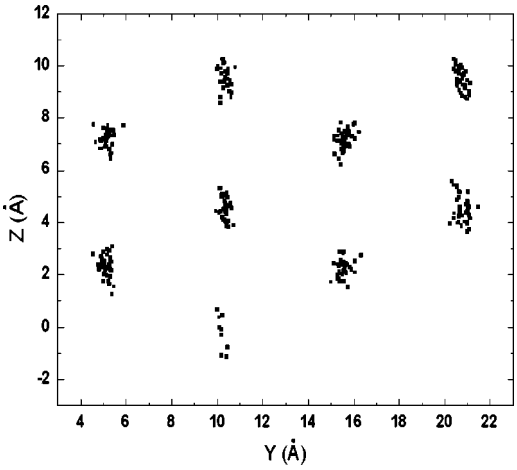

Figure 10. Snapshots of the movement of lithium atoms in the *YZ* planes.

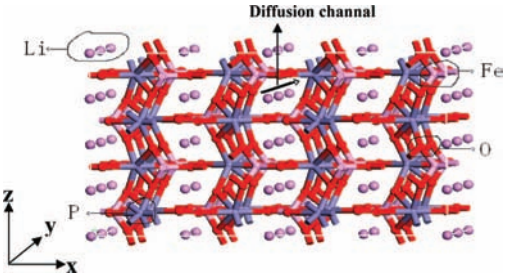

Figure 11. Olivine structure of a $LiFePO_4$ crystal and lithium ion migration paths along the *y* axis.

ditionally, this work shows that MD methods are capable of probing more mechanistic details at the microscopic level and offer a more direct approach to probe cooperative diffusion mechanisms.

Diffusion coefficients (D_{Li}) for $LiFePO_4$ have been calculated, which are on the order of 1.8×10^{-14} cm^2 s^{-1}. Chung et al.[6] showed experimentally that the electronic conductivity of $LiFePO_4$ could be increased enormously by substituting a small amount high valence metal ions for lithium ions. However, it seems that the enhanced electronic conductivity does not improve the electrochemical performance as expected. Given such a one-dimensional pathway, long-range Li conduction could be easily blocked. If the heavy high valence metal ions lie in the lithium sites, the one-dimensional diffusing pathway will be blocked. It appears that the electrochemical performance reported by Chung et al.[6] be limited by the slower process, Li ion diffusion. The conclusion can be confirmed theoretically by this study to the result of Chung et al.[6]

4. Conclusions

Molecular dynamics (MD) techniques have been employed to investigate the structure and transport properties of the ions in $LiFePO_4$. Conclusions drawn from this study can be summarized as follow:

(1) The radial distribution function indicates that the degree of disorder increases when the temperature increases as a higher temperature will enhance atoms diffusions. The information obtained from our studies can be used to estimate the structural parameter and melting point. The calculation shows good agreement with the experimental data.

(2) The msd of lithium becomes a constant after 10 ps, which suggests that further diffusion of lithium will not likely occur. The apparently large msd of lithium stems from relatively large displacements from their ideal positions.

(3) By analyzing the trajectories of the lithium ions, we found that the diffusion process is anisotropic and one-dimensionally along the channels parallel to the *b* axis. In the view of the type of one-dimensional mechanism, long-range lithium ions conduction could be blocked and this could affect the electrochemical performances during lithium extractions.

Acknowledgment. This work was financially supported by the National Natural Science Foundation of China (grant #50474092) and Shenzhen Government's Plan of Science and Technology (grant #200505)

References and Notes

(1) Padhi, A. K.; Nanjundaswamy, K. S.; Goodenough, J. B. *J. Electrochem. Soc.* **1997**, *144*, 1188.
(2) Takahashi, M.; Tobishima, S.; Takei, K.; Sakurai, Y. *Solid State Ionics* **2002**, *148*, 283.
(3) Padhi, A. K.; Nanjundaswamy, K. S.; Masquelier, C.; Okada, S.; Goodenough, J. B. *J. Electrochem. Soc.* **1997**, *144*, 1609.
(4) Andersson, A. S.; Thomas, J. O. *J. Power Sources* **2001**, *498*, 97–98.
(5) Ravet, N.; Chouinard, Y.; Magnan, J. F.; Besner, S.; Gauthier, M. *J. Power Sources* **2001**, *503*, 97–98.
(6) Chung, S.; Bloking, J. T.; Chiang, Y. *Nat. Mater.* **2002**, *1*, 123.
(7) Morgan, D.; Van der Ven, A.; Ceder, G. *Electrochem. Solid-State Lett.* **2003**, *7*, A30.
(8) Ouyang, C. Y.; shi, S. Q.; Wang, Z. X.; Li, H.; Huang, X. J.; Chen, L. Q. *J. Phys.: Condens. Matter* **2004**, *16*, 2265.
(9) Cygan, R. T.; Westrich, H. R.; Doughty, D. H. *Mater. Res. Soc. Proc* **1995**, *393*, 113.
(10) Ammundsen, B.; Roziere, J.; Islam, M. S. *J. Phys. Chem. B* **1997**, *101*, 8156.
(11) Suzuki, K.; Oumi, Y.; Takami, S.; Kubo, M.; Miyamoto, A.; Kikuchi, M.; Yamazaki, N.; Mita, M. *Jpn. J. Appl. Phys.* **2000**, *39*, 4318.
(12) Gotlic, I. Y.; Murin, I. V.; Piotrovskaya, E. M. *Inorg. Mater.* **2003**, *39*, 404.
(13) Lewis, G. V.; Catlow, C. R. A. *J. Phys. C: Solid State Phys.* **1985**, *18*, 1149.
(14) Tilocca, A.; Leeuw, N. H.; Alastair, N. C. *Phys. Rev. B* **2006**, *73*, 104209.
(15) Channon, Y. M.; Catlow, C. R. A.; Gorman, A. M.; Jackson, R. A. *Phys. Rev. B* **1998**, *102*, 4045.
(16) Islam, M. S.; Tolchard, J. R.; Slater, P. R. *Chem. Commun.* **2003**, *13*, 1486.
(17) Tolchard, J. R.; Islam, M. S.; Slater, P. R. *J. Mater. Chem.* **2003**, *13*, 1956.
(18) Leeuw, N. H.; Mkhonto, D. *Chem. Mater.* **2003**, *15*, 1567.
(19) Islam, M. S.; Driscoll, D. J.; Fisher, C. A.; Slater, J.; Peter, R. *Chem. Mater.* **2005**, *17*, 5085.
(20) Mitchell, P. J.; Fincham, D. *J. Phys: Condens. Matter* **1993**, *5*, 1031.
(21) Dick, R. G.; Overhauser, A. W. *Phys. Rev.* **1958**, *112*, 90.
(22) Forester, T. R.; Smith, W. *DL_POLY code*; Daresbury Laboratory, U.K., 1993.
(23) Rousse, G.; Rodriguez-Carvajal, J.; Patoux, S.; Masquelier, C. *Chem. Mater.* **2003**, *15*, 4082.
(24) Frenkel, D.; Smith, B. *Understanding Molecular Sinulation: From Algorithms to Applications*, 2nd ed.; New York, 2002.
(25) Tateishi, K.; Douglas, D. B.; Nobuo, I.; Katsuyuki, K. *J. Solid State Chem.* **2003**, *174*, 175.
(26) Dahn, J. R.; Von Sacken, U.; Michal, C. A. *Solid State Ionics* **1990**, *44*, 87.
(27) Goodenough, J. B. *Solid State Ionics* **1994**, *69*, 184.
(28) Ouyang, C. Y.; Shi, S. Q.; Wang, Z. X.; Li, H.; Huang, X. J.; Chen, L. Q. *J. Phys. Chem B* **2004**, *69*, 104303.

JP710204Z